Micromechanical testing for quantitative characterization of apparent slip system: Extinction of persistence of slip in carbon bearing Fe-3% Si

Tanaka, Masaki
Department of Materials, Faculty of Engineering, Kyushu University

Takenaka, Masanori
Steel Research Laboratory, JFE Steel Corporation

Yamasaki, Shigeto
Department of Materials, Faculty of Engineering, Kyushu University

Morikawa, Tatsuya
Department of Materials, Faculty of Engineering, Kyushu University

出版情報：Scripta Materialia. 232, pp.115473-, 2023-07-15. Elsevier
バージョン：

Scripta Materialia 232 (2023) 115473

Contents lists available at ScienceDirect

Scripta Materialia

journal homepage: www.journals.elsevier.com/scripta-materialia

Micromechanical testing for quantitative characterization of apparent slip system: Extinction of persistence of slip in carbon bearing Fe-3% Si

Masaki Tanaka [a,b,*], Masanori Takenaka [c], Shigeto Yamasaki [a], Tatsuya Morikawa [a]

[a] Department of Materials, Faculty of Engineering, Kyushu University, 744 Motooka, Nishi-ku, Fukuoka, 819-0395 Japan
[b] Center for Elements Strategy Initiative for Structural Materials (ESISM), Kyoto University, Sakyo-ku, Kyoto, 606-8501 Japan
[c] Steel Research Laboratory, JFE Steel Corporation, 1-chome Kawasakidori, Mizushima, Kurashiki, 712-8511 Japan

ARTICLE INFO

Keywords:
Silicon steel
Iron alloys
Slip
Plastic deformation
Dislocation

ABSTRACT

The effect of carbon on the persistence of the slip in Fe–3 mass% Si was investigated. We applied micro-sized cantilever bending tests to obtain ψ–χ relationships that enable quantitative analysis of the persistence of the slip. It was demonstrated that the result from decarburized specimens using this method is consistent with those obtained in previous studies from bulk-sized tensile test specimens. This novel method eliminates the difficulty of preparing bulk-sized single-crystal specimens for investigating the persistence of the slip. The persistence of the slip weakened in aged specimens containing 0.016 mass% C and disappeared in quenched specimens with the same carbon content, where wavy slip bands were observed. The reason for these changes in the macroscopically apparent slip plane is explained by the assumption that the frequency of nucleating kink-pair in the competitive {110} planes is a function of the resolved shear stress.

Electrical steel sheets are used for the core materials of motors and transformers. The conversion efficiency of electrical equipment deteriorates owing to iron losses caused by eddy current and hysteresis losses. One countermeasure to reduce eddy current loss is to add silicon; therefore, Fe–Si alloys are widely used for these electrical steel sheets [1–3]. A characteristic mechanical property of Fe–Si alloys is the persistence of the slip, which is observed as straight slip bands on a specimen surface after plastic deformation. In pure iron, wavy slip bands are generally observed on the specimen surface after plastic deformation—the so-called pencil glide [4,5]. It is reported, based on experimental data, that slip bands become straight on {110} plane as the silicon content in the iron increases [6–9]. In addition to silicon, other elements also influence the persistence of the slip. Takenaka et al. [10] investigated slip traces of tensile specimens after plastic deformation in detail using polycrystalline Fe–3 mass% Si with carbon contents of less than 0.0005 mass% and 0.016 mass%. They reported activation of multiple slip systems of the {110}, {112}, and {123} planes in the specimens with 0.016 mass% C; in contrast, slip persisted on the {110} planes in the specimens with the carbon content less than 0.0005 mass %. This result indicates that the presence of carbon in polycrystalline Fe–3 mass% Si weakens the persistence of the slip due to the enhancement of cross-slip. It is still ambiguous, however, whether the change in the persistence of the slip is due to the cementite or solute carbon in grains or those on grain boundaries. Therefore, it is essential to quantitatively determine the persistence of the slip.

However, studies on the persistence of slip have been limited [7-9, 11-15]. One reason for the lack of investigation of this phenomenon is the difficulty of specimen preparation because single crystals are required for the experiments. To overcome this difficulty, we applied a novel experimental method that uses micro-sized cantilever bending specimens fabricated using a focused ion beam to investigate the persistence of the slip, which enables single crystalline specimens having a different tensile direction to easily be obtained from a single grain of a polycrystalline specimen such as micro-pillar specimens [15–29]. In the present study, we determined the effect of carbon on the magnitude of persistence of the slip in Fe–3 mass% Si using micro-sized cantilevers. ψ–χ relationships which enable quantitative analysis of the persistence of the slip were obtained.

Here, the meaning of the ψ–χ relationship is briefly reviewed. Fig. 1 (a) shows a near-centre region on a [001] standard stereographic triangle. Supposing that the tensile direction is set in the direction marked × in the standard stereographic triangle, the slip direction determined as the [111] direction. With this geometry, it is expected that the slip plane would be one of the planes in the great circle connecting the $[\bar{1}\bar{1}2]$ and

* Corresponding author.
E-mail address: masaki@zaiko.kyushu-u.ac.jp (M. Tanaka).

https://doi.org/10.1016/j.scriptamat.2023.115473
Received 26 November 2022; Received in revised form 19 March 2023; Accepted 4 April 2023
Available online 13 April 2023

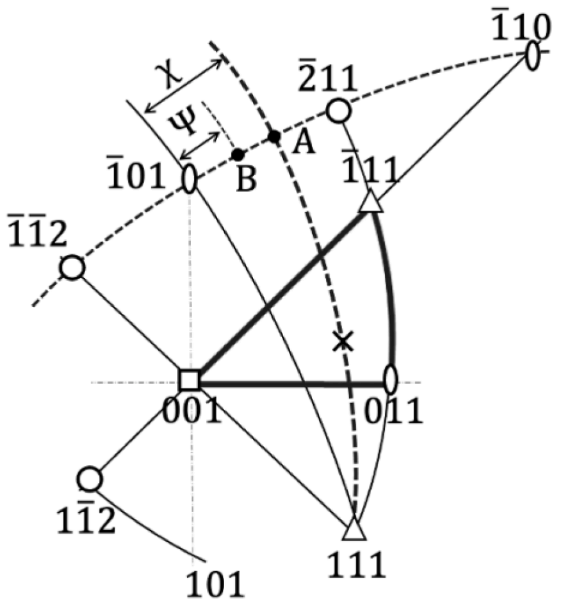

Fig. 1. Schematic drawing of ψ–χ relationship in a standard stereographic triangle. Point × indicates the tensile direction. The [111] direction is the slip direction. Capital letter A indicates the maximum shear stress plane; Capital letter B indicates the apparent slip plane.

$[\bar{2}11]$ directions. The plane with the highest resolved shear stress is denoted as A in Fig. 1(a). Plane A is called the maximum shear stress plane (MSSP). Here, the angle between the MSSP and the $(\bar{1}01)$ plane is defined as χ. The angle between the apparent slip plane and the $(\bar{1}01)$ plane is defined as ψ. The signs of ψ and χ are defined as positive when MSSP and the macroscopically apparent slip planes are between the $(\bar{1}01)$ plane and the $(\bar{2}11)$ plane, and as negative when they are between the $(\bar{1}01)$ plane and the $(\bar{1}\bar{1}2)$ plane. The result of $\psi = \chi$ indicates that the MSSP and the macroscopically apparent slip planes are identical; hence, the slip planes are not persistent and dislocations frequently cross-slip. The result of $\psi \neq \chi$ indicates that slip planes persist and cross-slip is suppressed. Here, it is to be noted that the macroscopically apparent {112} slip planes, and other non {110} slip planes are formed with the combination of two different {110} planes from an atomistic point of view.

We used 3 mass% Si steel containing 0.016 mass% C annealed at 1273 K for 60 s after hot rolling as the starting material. The material was cold rolled with a reduction of 25% after the annealing. The following heat treatments were applied to the starting material to obtain three types of test specimens. The specimen denoted as ULC (ultralow carbon) was quenched into ice water after recrystallization at 1373 K for 300 s, followed by decarburization at 1023 K for 18 ks. The carbon content of ULC after the decarburization was less than 0.0005 mass%. The second specimen, denoted as CA (carbon-bearing with ageing), contained 0.016 mass% C in 3 mass% Si steel and was annealed at 673 K for 86.4 ks and cooled in the furnace to promote cementite to precipitate coarsely followed by quenching into ice water after recrystallization at 1373 K for 300 s. The third specimen, denoted as CQ (carbon-bearing with quenching), contained 0.016 mass% C in 3 mass% Si steel and was quenched into ice water after recrystallization at 1373 K for 300 s.

Crystal orientations were determined using electron backscatter diffraction (EBSD) and used to choose appropriate grains to make micro-sized cantilevers which were fabricated using a focused ion beam. The cantilever size is shown in Fig. 2(a), where the length, width, and thickness of the cantilevers were 15, 7, and 4 μm, respectively. Several cantilevers were cut from within the grain in different longitudinal orientations, as shown in Fig. 2(b). In the bending tests, the edge of the cantilever was pushed by a flat-punch-type indenter at room

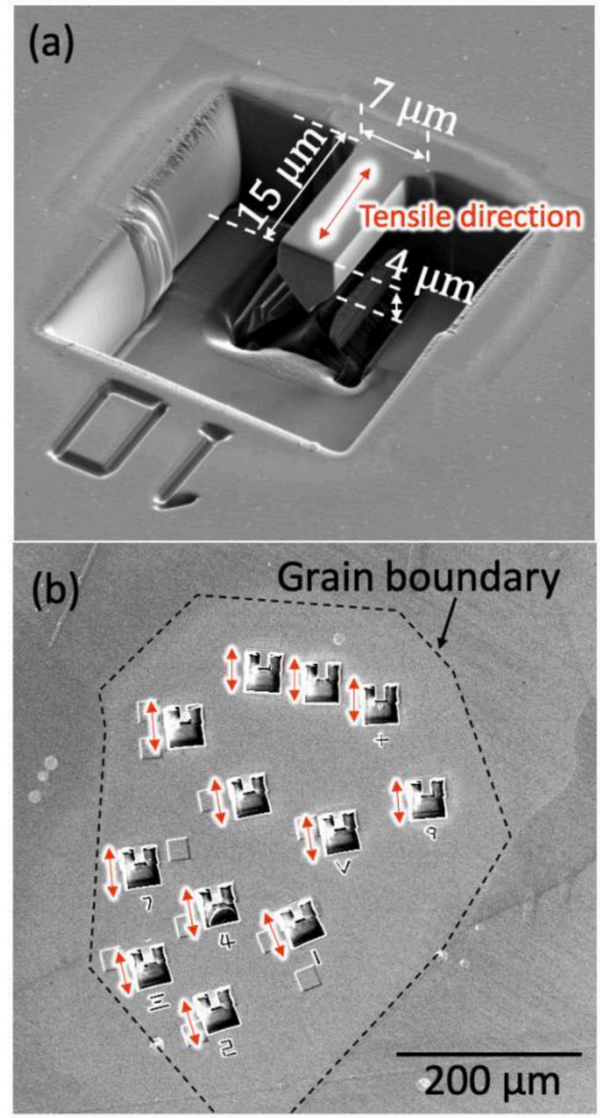

Fig. 2. (a) Enlarged image of a micro-sized cantilever. Tensile direction on the top surface and standard specimen dimensions are denoted. (b) Micro-sized cantilevers within a grain. Several cantilevers were fabricated within a grain, where red arrows show different longitudinal directions of the cantilevers to be investigated.

temperature to apply tensile stress on the top surface of the cantilever with a nano-indentation tester. The indenter tip moved down 1.5 μm after contact with the cantilever at a rate of 15 nm/s. The slip traces were observed using SEM and their directions were analysed with EBSD patterns.

Fig. 3(a)–(c) show top views of scanning electron microscopy images of the micro-sized cantilevers after bending tests for ULC, CA, and CQ. The root of the cantilever locates the right side of each image. The vertical marking remaining on the cantilever surface at the near left edge results from contact with the flat-punch-type indenter. As the flat-patch indenter is not a prism but a truncated square pyramid, the ridge of the pyramid of the indenter digs into the sample during the loading. Slip traces are shown as yellow lines in Fig. 3. The values of ψ were determined from slip traces which were located the furthest distance from the cantilever root to avoid a complex stress state near the cantilever root. It is reasonable to assume that slip deformation occurs under uniaxial tensile stress on the top region of the cantilever far from the root. The values of ψ of the specimens in Fig. 3 were determined as 14°, 16°, and 23° for ULC, CA, and CQ, respectively. These results suggest that the

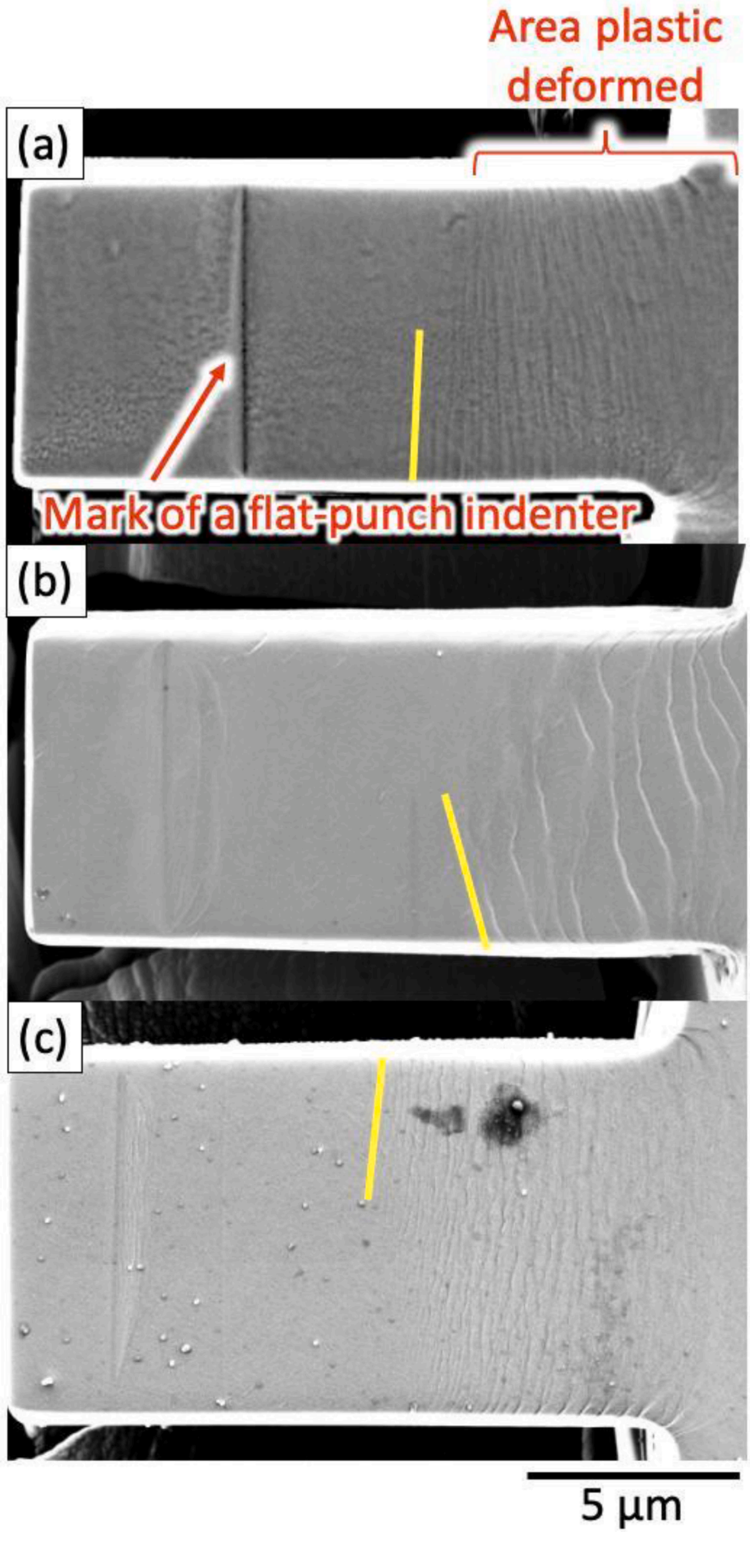

Fig. 3. Top views of scanning electron micrographs of micro-sized cantilevers after bending tests. Yellow lines are the slip traces used to determine the value of ψ. (a) ULC and $\chi = -12^{\circ}$, (b) CA and $\chi = 21^{\circ}$, and (c) CQ and $\chi = 21^{\circ}$

persistence of the slip is the strongest in ULC, and the weakest in CQ. Actually, the slip traces were straight in ULC, as shown in Fig. 3(a), while they tend to be wavier in CA and CQ as shown in Fig. 3(b) and (c). In order to investigate the magnitude of the persistence of the slip quantitatively, ψ–χ relationships were obtained for different tensile directions within each specimen.

Fig. 4(a), (b), and (c) show the ψ–χ relationships obtained from ULC, CA, and CQ, respectively. The horizontal axis indicates χ, i.e., the angle between the $(\bar{1}01)$ plane and the MSSP; the vertical axis indicates ψ, i.e., the angle between the $(\bar{1}01)$ plane and the apparent slip plane. As mentioned previously, the deviation of |ψ| from |χ| indicates the magnitude of the persistence of the slip. Fig. 4(a) shows that $|\psi| < |\chi|$ for $-25^{\circ} < \chi < 25^{\circ}$ in the ULC specimen, indicating that the slip

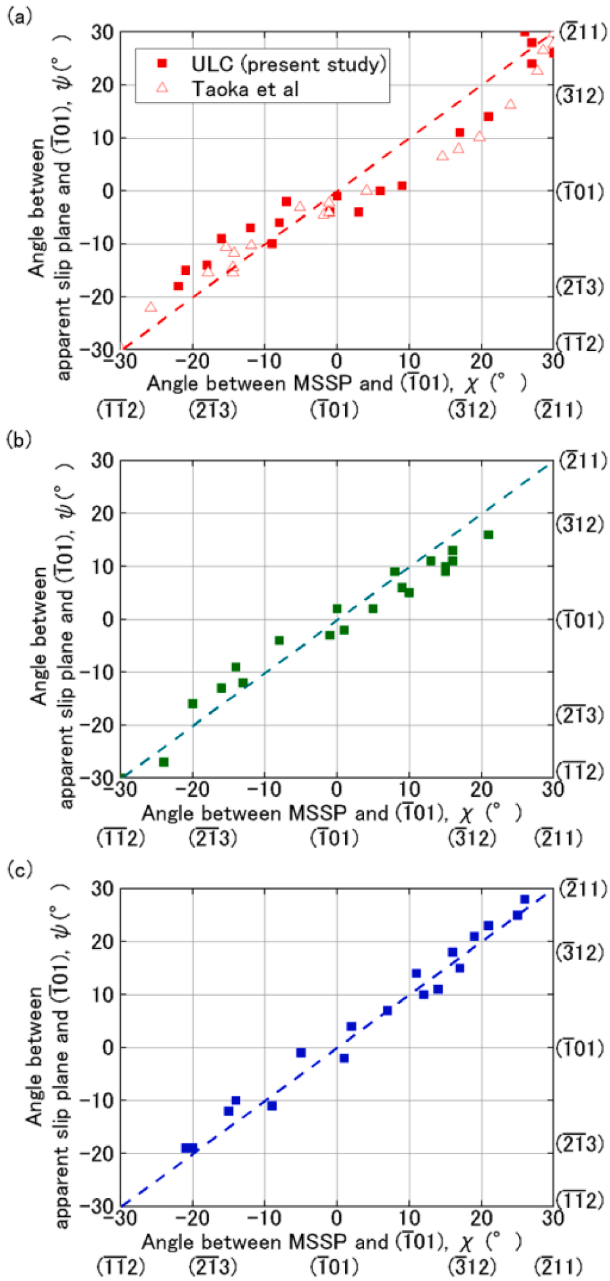

Fig. 4. ψ–χ relationships obtained from micro-sized cantilever bending tests. The straight lines in the figure indicate ψ = χ. (a) ULC, including results of bulk-sized single crystals from Taoka et al. [9], (b) CA, (c) CQ.

plane persisted on the $(\bar{1}01)$ planes. The magnitude of the persistence of the slip is stronger for 0° < χ (anti-twinning direction) than that for χ < 0° (twinning direction). This result is good agreement with that obtained for bulk-sized single crystalline Fe–3 mass% Si [9], the data for which are superimposed in Fig. 4(a). This good agreement demonstrates that the micro-sized cantilever bending tests gave identical results to those obtained for bulk-sized single crystals. Note, the ψ - χ relationships were obtained assuming the state of the stress is a simple uniaxial tensile stress along the micro-cantilever owing to the following reasons. (i) FEM model reflecting the experimental cantilever shape shows that the first principal stress on the top surface of the cantilever has tensile stress along the cantilever except for near the root of the cantilever. (ii) Slip bands which are the furthest from the notch root were used for the determination of ψ to minimise the influence of the complexity of the stress state due to the notch root. (iii) The ψ - χ relationship obtained in this study in Fig. 4(a) is consistent with that obtained from regular tensile tests.

Fig. 4(b) shows that plots of ψ were located closer to the line of ψ = χ than those in Fig. 4(a), which indicates that the magnitude of the persistence of the slip on the $(\bar{1}01)$ plane in CA is weaker than that in ULC. Fig. 4(c) shows that the plots of ψ are located almost on the line of ψ = χ for the entire range of χ, which indicates that the slip plane and MSSP are identical, i.e., slip does not persist on the {110} planes at all. As mentioned, it is reported that the magnitude of the persistence of the slip depends on the amount of solute silicon. The heat treatments applied in this study should not influence the state of the solute silicon because the temperature was low enough. Therefore, it is expected that the change in the magnitude of the persistence of the slip is related to the differences in the state of carbon in the specimens.

Fig. 5(a)–(c) show bright-field transmission electron micrographs from ULC, CA, and CQ, respectively, prior to bending tests. ULC had no cementite resulting from the well decarburizing. It is regarded that ULC rarely contains solute carbon. CA had coarsely precipitated cementite plates with a width of approximately 100 nm, suggesting CA also rarely contains solute carbon. CQ had densely distributed spherical cementite with a diameter of less than 20 nm. This morphology of the cementite indicates that the carbon was not completely supersaturated after quenching and precipitated as fine spherical cementite [30,31]. It is also assumed that CQ contains a large number of solute carbons.

Here, we discuss the reason why the magnitude of persistence of the slip is in the order of ULC > CA > CQ, i.e., how the state of the carbon influences the persistence of the slip. Although some models have been presented [8,32,33], the mechanism behind the enhancement of the persistence of the slip by addition of silicon itself has not yet been clarified. It is to be noted that even macroscopically apparent slip planes are such as {112}, {123}, or others, the slip planes were formed with the combination of competitive {110} planes atomistically. Monte carlo molecular dynamics simulation shows that the persistence of the slip is due to the formation of cross-kink, where kink-pair formed on different {110} planes meet and extinguish with forming a vacancy or interstitial atoms [34,35]. When applying this model to the present case, the existence of cementite should rather decrease the frequency of the formation of cross-kink to explain the experimental results that the persistence of the slip is supressed, i.e., more frequent cross-slips, by the cementite. However, cementite does not influence the thermally activated process of kink-pair nucleation, so that the existence of cementite should not influence the formation of kinks as the thermally activated process. Therefore, the cross-kink model is hard to explain the results obtained in this study.

The experimental data obtained in this study can be explained by the assumption that the persistence of the slip is a function of the effective shear stress. Edagawa et al. [36] analytically showed that the frequency of kink-pair nucleation among the competitive {110} plane is a function of the effective stress. They showed that the change rate of the potential with shear stress depends on the direction of the applied shear stress, resulting that the frequency of the kink-pair nucleation depends on the effective shear stress as a thermally activated process. If the effective stress is small, the difference in the frequency of the kink-pair nucleation in two competitive {110} planes is small, resulting in a small difference in the corresponding kink-pair nucleation probabilities among those {110} planes. On the contrary, if the effective stress is large, the difference in the frequency of the kink-pair nucleation in competitive {110} planes is large, resulting in a large difference in the corresponding kink-pair nucleation probabilities in competitive {110} planes. If the level of the effective stress is as the order of CQ (carbon-bearing with quenching) < CA (carbon-bearing with ageing) < ULC (ultralow carbon), it can explain the experimental results.

Here we briefly discuss the effect of interstitial carbons on the persistence of the slip. Nakanishi et al. [37] reported, with silicon-free steels, that the microstructure of cold-rolled low-carbon steel is

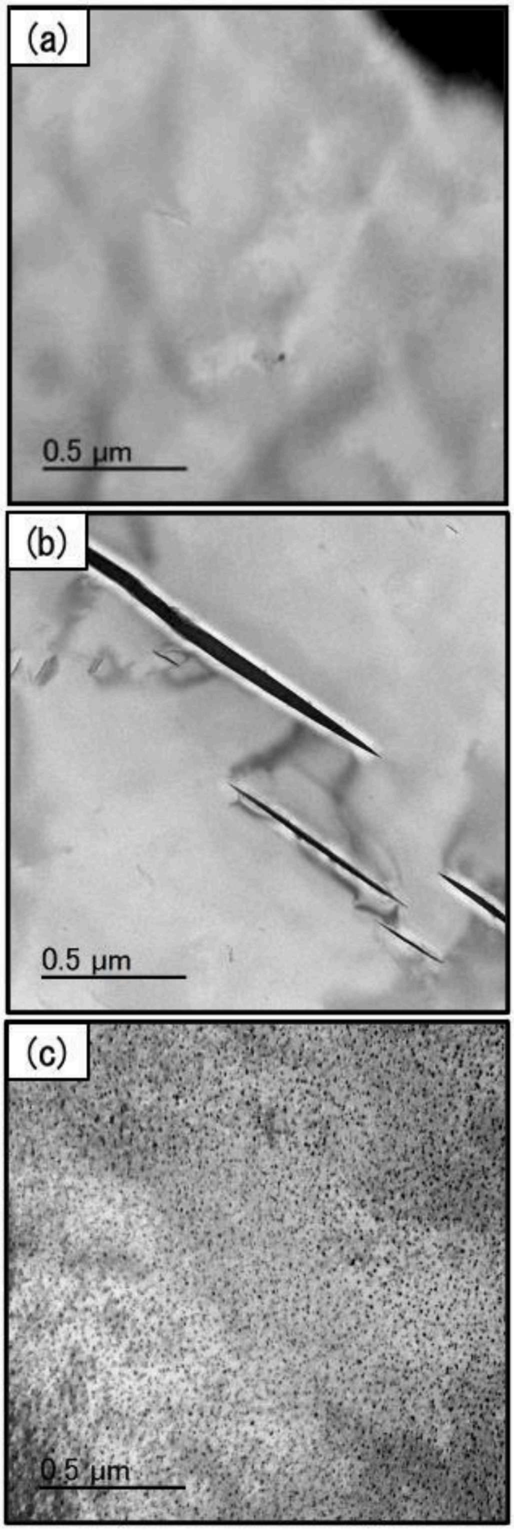

Fig. 5. Bright-field transmission electron micrographs prior to bending tests of (a) ULC, (b) CA, and (c) CQ.

different from those of Ti-added ultralow-carbon steel which is expected to be interstitial-carbon free. They showed TEM images of dislocation microstructures of deformed grains having the same orientation seen from a transverse direction after 70% in thickness reduction by cold rolling, demonstrating that dislocation cells grew in Ti-added ultralow-carbon steel while ambiguous dislocation cells grew in low-carbon steel. These suggest that the frequency of cross slip is higher in Ti-added ultralow-carbon steel than that in low-carbon steel, that is, solute carbons seem to suppress the frequency of cross slip. However, it is considered that Ti-added ultralow-carbon steel contains TiC, so it is necessary to have further experiments to obtain ψ–χ relationships of low-carbon steels with different interstitial carbon atoms to distinguish the effects of solute C and solute Si on the persistency of the slip in Fe.

In conclusion, it was demonstrated that the micro-sized cantilever bending is a novel method to investigate the persistence of the slip and the results are consistent with those obtained by conventional measurements using bulk-sized single crystals. The method described in this study has the advantage that single crystals are not necessary for the study. It was also determined from the ψ–χ relationships obtained by micro-sized cantilever bending that the magnitude of the persistence of the slip is the strongest in a decarburized Fe–3 mass% Si and weakest in quenched carbon bearing Fe–3 mass% Si. The weakening of the persistence of the slip in the carbon bearing Fe–Si alloys can be explained by the assumption that the frequency of nucleating kink-pair in the competitive {110} planes is a function of the resolved shear stress.

Declaration of Competing Interest

The authors declare that they have no known competing financial interests or personal relationships that could have appeared to influence the work reported in this paper.

References

[1] J. Yang, Z.W. Fu, J.H. Ye, D. Kubrich, C. Korner, Electron beam-based additive manufacturing of $Fe_{93.5}Si_{6.5}$ (wt.%) soft magnetic material with controllable magnetic performance, Scr. Mater. 210 (2022), 114460.
[2] F. Ismagilov, V. Vavilov, A. Zherebtsov, A. Miniyarov, E. Pronin, Obtaining a dual-phase magnetic material based on electrical silicon steel sheet, J. Mag. Mag. Mater. 557 (2022), 169457.
[3] Y. Guo, F.Q. Dai, X.C. Zeng, Numerical simulation of decarburization kinetics for Fe-3%Si steel during annealing, ISIJ Int. 59 (2019) 326–335.
[4] G.I. Taylor, C.F. Elan, The distortion of iron crystals, Pro. Roy. Soc. Lon. A 112 (1926) 337–361.
[5] L.T. Le, K. Ammar, S. Forest, Efficient simulation of single and poly-crystal plasticity based on the pencil glide mechanism, Comptes Rendus Mécanique 348 (2020) 847–876.
[6] S. Libovický, B. Šesták, Influence of the silicon content on the crystallography of slip in iron—Silicon alloy single crystals, J. App. Phys. 34 (1963) 2919–2921.
[7] B. Šesták, N. Zarubova, Asymmetry of slip in Fe-Si alloy single crystals, Phys. Stat. Sol.(b) 10 (1965) 239–250.
[8] S. Takeuchi, E. Furubayashi, T. Taoka, Orientation dependence of yield stress in 4.4% silicon iron single crystals, Acta Metall. 15 (1967) 1179–1191.
[9] T. Taoka, S. Takeuchi, E. Furubayashi, Slip systems and their critical shear stress in 3% silicon iron, J. Phys. Soc. Jpn. 19 (1964) 701–711.
[10] M. Takenaka, N. Fujita, Y. Hayakawa, N. Tsuji, Unique effect of carbon addition on development of deformation texture through changes in slip activation and twin deformation in heavily cold-rolled Fe-3% Si alloys, Acta Mater. 157 (2018) 196–208.
[11] C.D. Statham, D. Vesely, J.W. Christian, Slip in single crystals of niobium-molybdenum alloys deformed in compression, Acta Metall. 18 (1970) 1243–1251.
[12] K. Edagawa, T. Suzuki, S. Takeuchi, Plastic anisotropy in b.c.c. transition metals, Mater. Sci. Eng. A234-236 (1997) 1103–1105.
[13] W.A. Spitzig, A.S. Keh, Orientation and temperature dependence of slip in iron single crystals, Metall. Trans. 1 (1970) 2751–2757.
[14] H. Saka, G. Taylor, Slip systems in a body-centred-cubic Li—Mg alloy, Philos. Mag. A 43 (1981) 1377–1392.
[15] M. Tanaka, S. Okajo, S. Yamasaki, T. Morikawa, Persistent slip observed in TiZrNbHfTa: a body-centered high-entropy cubic alloy, Scr. Mater. 200 (2021), 113895.
[16] K. Chu, Q. Sun, Reducing functional fatigue, transition stress and hysteresis of NiTi micropillars by one-step overstressed plastic deformation, Scr. Mater. 201 (2021), 113958.
[17] K. Chou, O. Neill, E.A. Marquis, Oxygen-induced refinement of α precipitates in an aged metastable β Ti-15-333 alloy, Scr. Mater. 205 (2021), 114206.
[18] Y.F. Zhang, R. Su, T.J. Niu, N.A. Richter, S. Xue, Q. Li, J. Ding, B. Yang, H. Wang, X. Zhang, Thermal stability and deformability of annealed nanotwinned Al/Ti multilayers, Scr. Mater. 186 (2020) 219–224.
[19] W. Roberts, J. Gong, A.J. Wilkinson, E. Tarleton, Tension-compression asymmetry of < c plus a >slip in Ti-6Al, Scr. Mater. 178 (2020) 119–123.
[20] N.G. Mathews, A.K. Saxena, C. Kirchlechner, G. Dehm, B.N. Jaya, Effect of size and domain orientation on strength of Barium Titanate, Scr. Mater. 182 (2020) 68–73.
[21] J. Li, W. Lu, J. Gibson, S. Zhang, S. Korte-Kerzel, D. Raabe, Compatible deformation and extra strengthening by heterogeneous nanolayer composites, Scr. Mater. 179 (2020) 30–35.

[22] B.S. Li, T.J. Marrow, D.E.J. Armstrong, Measuring the brittle-to-ductile transition temperature of tungsten-tantalum alloy using chevron-notched micro-cantilevers, Scr. Mater. 180 (2020) 77–82.

[23] S.I.A. Jalali, P. Kumar, V. Jayaram, Microstructural equivalence between bending and uniaxial creep, Scr. Mater. 186 (2020) 99–103.

[24] N.L. Okamoto, M. Inomoto, H. Adachi, H. Takebayashi, H. Inui, Micropillar compression deformation of single crystals of the intermetallic compound ζ-FeZn13, Acta Mater 65 (2014) 229–239.

[25] A. Shibata, T. Nagoshi, M. Sone, S. Morito, Y. Higo, Evaluation of the block boundary and sub-block boundary strengths of ferrous lath martensite using a micro-bending test, Mater. Sci. Eng. A 527 (2010) 7538–7544.

[26] T.Y. Sun, J. Cho, Z.X. Shang, T.J. Niu, J. Ding, J. Wang, H.Y. Wang, X.H. Zhang, Deformation mechanism in nanolaminate FeCrAl alloys by in situ micromechanical strain rate jump tests at elevated temperatures, Scr. Mater. 215 (2022), 114698.

[27] K.J. Chu, Q.P. Sun, Reducing functional fatigue, transition stress and hysteresis of NiTi micropillars by one-step overstressed plastic deformation, Scr. Mater. 201 (2021), 113958.

[28] K.X. Li, Y.L. Zhuang, L.G. Zhao, D.S. Zhao, H. Zheng, S.F. Jia, Y. Zhang, P.L. Zhao, J.N. Gui, J.B. Wang, In-situ observation of the interaction of {1012}a deformation twinning with 18R long period stacking ordered precipitates in an Mg-5Gd-3.5Ga (at.%) as-cast alloy, Scr. Mater. 210 (2022), 114392.

[29] P. Hua, H. Lin, Q. Sun, Ultrahigh cycle fatigue deformation of polycrystalline NiTi micropillars, Scr. Mater. 203 (2021), 114108.

[30] K. Ushioda, K. Takata, J. Takahashi, K. Kinoshita, H. Sawada, Changes in states of carbon and mechanical properties with aging at 50 °C after quenching in low carbon steel, Mater. Trans. 61 (2020) 668–677.

[31] T. Shimokawa, K. Yasui, T. Niiyama, K. Kinoshita, H. Sawada, A mechanism of carbon-cluster strengthening through atomic simulations, Mater. Trans. 61 (2020) 2139–2148.

[32] A.W. Sleeswyk, 1/2<111>screw dislocations and the nucleation of {112}<111>twins in the b.c.c. lattice, Philos. Mag. 8 (1963) 1467–1468.

[33] C.N. Reid, A. Gilbert, G.T. Hahn, Twinning, slip and catastrophic flow in niobium, Acta Metal. 14 (1966) 975–983.

[34] T. Mohri, Y. Chen, M. Kohyama, S. Ogata, A. Saengdeejing, S.K. Bhattacharya, M. Wakeda, S. Shinzato, H. Kimizuka, Mechanical properties of Fe-rich Si alloy from Hamiltonian, NPJ Comput. Mater. 3 (2017), 10.

[35] S. Shinzato, M. Wakeda, S. Ogata, Theoretical prediction of macroscopic yield strength for Fe alloy based on atomistic study, J. Jpn. Inst. Met. 80 (2016) 197–205.

[36] E. Edagawa, T. Suzuki, S. Takeuchi, Motion of a screw dislocation in a two-dimensional Peierls potential, Phy. Rev. B 55 (1997) 6180–6187.

[37] S. Nakanishi, T. Morikawa, K. Higashida, H. Murakami, K. Kimura, K. Ushioda, Effect of solute carbon content on microstructure of cold-rolled ferritic steel - The same area analyses by using TEM and SEM-EBSD-, Tetsu-to-Hagané 98 (2012) 253–261.